




Cite this: *J. Mater. Chem. B*, 2022, 10, 958

Highly effective gene delivery based on cyclodextrin multivalent assembly in target cancer cells†

Yao-Hua Liu and Yu Liu *

Nucleic acid condensation and controlled release remain significant challenges of gene therapy in the fields of chemical biology and nanotechnology. In this work, we have reported a polysaccharide supramolecular assembly constructed using upconversion nanoparticles encapsulated by β -cyclodextrin-grafted hyaluronic acid (HACD-UCNPs) and spermine modified with arylazopyrazoles (AAPS). Through UV-Vis spectroscopy, transmission electron microscopy (TEM), dynamic light scattering (DLS), gel electrophoresis, confocal laser imaging and combination experiments, such an assembly can achieve not only nucleic acid condensation but also targeted cells delivery and controlled release. Furthermore, we investigated the ability of the system to deliver siRNA under hypoxic conditions, and the subsequent NIR irradiation regulation achieved the two-step release of RNA, obtaining the best effect. This strategy provides a new approach for nucleic acid condensation and targeted delivery, which may bring broad potential in gene therapy.

Received 23rd November 2021,
Accepted 3rd January 2022

DOI: 10.1039/d1tb02585f

rsc.li/materials-b

Introduction

The gene delivery system based on supramolecular chemistry has been a research hotspot in recent years as it can manipulate the corresponding molecule leading to a change in the biological function of the whole supramolecular system.^{1,2} Generally, this supramolecular system is fabricated *via* the combination of specific molecular–nucleic acid recognition and cooperative host–guest complexation.³ The introduction of additional functional molecules and dynamic host–guest interactions provides opportunities to regulate the structure and biological function of both the nucleic acid (NA) and the nucleic acid complex.^{4,5} In recent years, lots of nanosystems based on supramolecular assembly have been constructed for effective NA delivery.^{6,7} In particular, benefitting from the good water solubility, biocompatibility and extensive recognition ability of cyclodextrins (CDs), supramolecular delivery systems using CDs as building blocks have been widely favored by researchers.^{8,9} For example, Davis and co-workers reported a supramolecular nanoparticle based on small interfering RNA (siRNA) and the CD–adamantane complex for RNA interference (RNAi), which was the first example using supramolecular assemblies for siRNA delivery in clinical applications.¹⁰

Sollogoub, Bouteiller and co-workers reported a supramolecular polymer based on cationic cyclodextrin that can achieve DNA compaction or interact with siRNA and allow its transfection.¹¹ So far, CD systems for NA delivery have made great progress, proving the feasibility of the supramolecular system for gene delivery and its potential clinical application.

Furthermore, the introduction of stimuli-responsive sites into supramolecular systems can be used as a feasible strategy to fabricate intelligent nanocarriers, which can adapt and respond to microenvironmental variations leading to precise release.^{4,12,13} In this regard, azo-compounds are considered as building blocks for the construction of stimulus-responsive supramolecular nanocarriers because they show significant differences in binding affinities with CDs upon photoisomerization and reduction,^{14–17} which provides opportunities for the reversible capture and release of drug molecules¹⁸ and biomacromolecules.^{19,20} Moreover, those supramolecular systems containing azo compounds can be regulated *via* near infrared light (NIR) *via* the addition of photon upconversion nanoparticles, which cause less damage to healthy cells or living tissues and have deep tissue penetration, ensuring easy operability in biological environments.^{21,22}

Along with this idea, to achieve the controllable release of nucleic acids in targeted cells, we have constructed a dual-responsive supramolecular assembly for targeted nucleic acid release in two steps under the stimulation of reducing conditions and NIR light. Through combined experiments of UV-Vis spectroscopy, transmission electron microscopy (TEM), dynamic light

College of Chemistry, State Key Laboratory of Elemento-Organic Chemistry, Nankai University, Tianjin 300071, China. E-mail: yuliu@nankai.edu.cn

† Electronic supplementary information (ESI) available. See DOI: 10.1039/d1tb02585f

scattering (DLS), and gel electrophoresis, it is confirmed that the supramolecular assembly can effectively compress DNA and release it under stimulus-response conditions. Notably, after plasmid DNA that contains the enhanced green fluorescent protein gene (pEGFP) has been carried by the supramolecular assembly into cancer cells, it can effectively express only under the stimulation of light and intracellular reductase. By analogy, RNA interference caused by the assembly of (AAPS \subset HACD-UCNPs)@siRNA can only be achieved through culturing cells with light irradiation and under anaerobic conditions. Benefitting from the specific recognition of receptors overexpressed on the cell membrane of cancer cells, the supramolecular assembly loaded with nucleic acids did not enter the normal cells. Therefore, this supramolecular system can compress nucleic acids forming nanoparticles, and achieve precise release in targeted cancer cells, which provide a universal strategy for building a stimulus-responsive platform of effective gene delivery.

Experimental section

Reagents and materials

All chemicals were of commercially available reagent grade and were used without further purification, unless otherwise noted. HACD²³ (the degree of modification of β -cyclodextrin was about 35%), UCNPs,²⁴ the Boc-protected spermine⁵ and AAPS¹⁴ were prepared according to the reported literature procedure. The plasmid DNA (pBR322) was purchased from Thermo Fisher Scientific. The pEGFP (mammalian cell expression plasmid, used to express N-terminal fusion protein containing EGFP) was purchased from Shanghai Beyotime Co., Ltd. The siRNA (GAPDH-homo), Cy5-siRNA (Cy5 labeled siRNA) and negative control siRNA (c-siRNA) were purchased from Shanghai GenePharma Co., Ltd. The sequences of siRNA are shown as follows: sense UGA CCU CAA CUA CAU GGU UTT and anti-sense AAC CAU GUA GUU GAG GUC ATT. The initial concentration of siRNA was 5 μ M (dissolved in dH₂O).

Synthesis of HACD-UCNPs

5 mL of UCNPs cyclohexane solution and 5 mL of HACD aqueous solution were mixed in a 25 mL single-necked bottle. After vigorous stirring overnight, the liquids were separated to obtain the water phase. After washing the aqueous phase twice with cyclohexane, the water phase was lyophilized and dissolved in 5 mL PBS (0.01 M, pH = 7.2) solution to obtain 1 mM HACD-UCNPs solution (the concentration was calculated as β -cyclodextrin).

Synthesis of AAPS

AAP (823.42 mg, 3.19 mmol) and PyBop (1.99 g, 3.83 mmol) were dissolved in dry DMF (50 mL). The solution was purged with argon gas three times and then stirred for 30 min. Next, *N,N*-diisopropylethylamine (1.67 mL, 9.56 mmol) and Boc-protected spermine (0.95g, 3.83 mmol) were added to the reaction mixture with constant stirring. The solution was stirred overnight at room temperature under argon. The solvent was removed under reduced pressure. The residue was dissolved in ethyl acetate,

washed with brine and water. The organic phase was dried over Na₂SO₄, and the solvent was removed under reduced pressure. Purification using column chromatography (DCM/CH₃OH 50 : 1) yielded the Boc-protected AAPS as a yellow oil. The Boc-protected AAPS was dissolved in methanol (50 mL) and acetyl chloride (2 mL) was added slowly at 0 °C. Then the solution was stirred overnight at room temperature. Evaporation of the solvent yielded AAPS as a yellow solid (568 mg, 1.03 mmol, 32%).

¹H NMR: (400 MHz, D₂O) δ = 7.76 (d, *J* = 7.3 Hz, 2H), 7.56–7.47 (m, 3H), 4.85 (s, 2H), 3.34 (t, *J* = 6.5 Hz, 2H), 3.08–3.00 (m, 10H), 2.51 (s, 3H), 2.42 (s, 3H), 2.06–1.99 (m, 2H), 1.93–1.86 (m, 2H), 1.71 (s, 4H) ppm. ¹³C NMR (101 MHz, D₂O) δ = 169.23, 152.54, 141.55, 134.40, 130.33, 129.21, 121.45, 50.68, 46.92, 46.80, 44.93, 44.43, 36.39, 36.16, 25.55, 23.65, 22.69, 22.62, 12.58, 9.04 ppm. MS (*m/z*): (ESI, H₂O) calculated for [M – 3HCl + H]⁺: 443.32, found 443.33.

Preparation of ternary supramolecular assembly (AAPS \subset HACD-UCNPs@NAs)

The stock solutions of AAPS \subset HACD-UCNPs@NAs were prepared by dissolving 0.55 mg of AAPS (1 mmol) in 1 mL of HACD-UCNPs solution (1 M). Next, different amounts of NA solution were mixed with the above solution. Then, the solution was homogenized using ultrasound for 5 min and stored at 4 °C for further use.

Agarose gel electrophoresis

Agarose gel electrophoresis experiments were performed in TAE buffer (0.04 M Tris, 0.02 M acetic acid, and 2.0 mM ethylenediaminetetraacetic acid (EDTA)) at 25 °C. Various samples in 5 mL loading buffer were mixed with 100 ng of plasmid pBR322 in 5 mL loading buffer, and the mixtures were incubated at 37 °C for 30 min. Following electrophoresis, plasmid pBR322 bands were stained using a GelRed solution and were visualized under UV light at 302 nm.

DNA transfection *in vitro*

Cells were seeded in a glass-bottomed dish for 24 h at 37 °C in 5% CO₂. The pre-configured supramolecular assembly solution of AAPS \subset HACD-UCNPs@pEGFP was diluted with culture medium containing 10% FBS, and the complex solutions were incubated for 30 min at 37 °C. The cells were incubated with complexes for 12 h (1.6 μ g pEGFP per well). The cells were further incubated for 24 h. Then the dishes were observed using a confocal microscope.

RNA transfection *in vitro*

A549 and 293T cells were seeded in a glass-bottomed dish for 24 h at 37 °C in 5% CO₂. The pre-configured supramolecular assembly solution of AAPS \subset HACD-UCNPs@Cy5-siRNA was diluted with culture medium containing 10% FBS, and the complex solutions were incubated for 30 min at 37 °C. The cells were incubated with complexes for 12 h (the concentration of siRNA was 100 nM). The cells were further incubated for 24 h. Then the dishes were observed using a confocal microscope.

In vitro cytotoxicity tests

To investigate the toxicity of AAPS, HACD-UCNPs, and their complexes with siRNA to cells, the cells were cultured in 96-well plates in corresponding medium containing 10% FBS for 24 h, and then the corresponding samples were added into the wells. The cells were further cultured for 24 h, and then the cell viability was examined using a CCK-8 assay kit (NCM Biotech, China).

Anaerobic culture

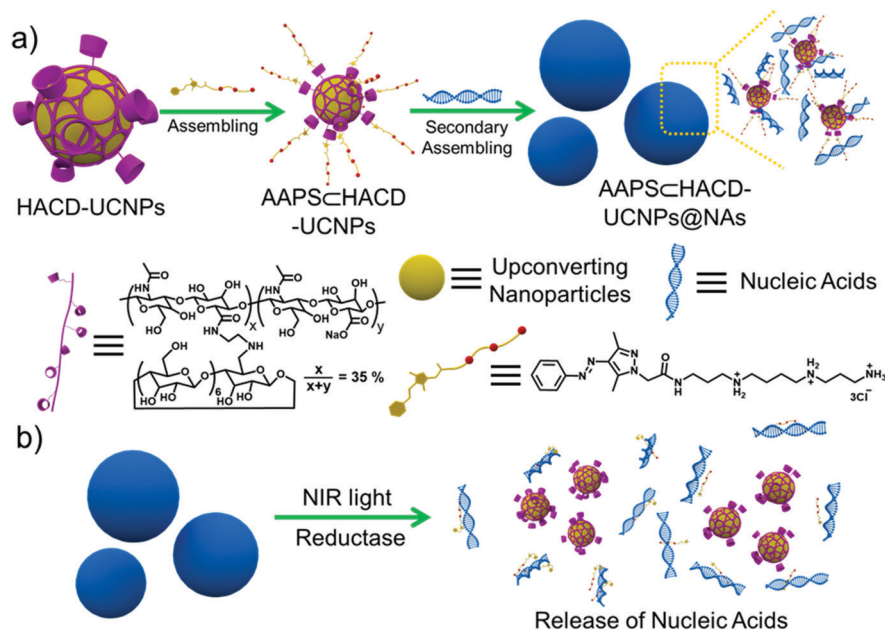
Anaerobic culture of cells was used using a Pouch-Bag and AnaeroPack-Anaero equipment (Mitsubishi Gas Chemical Company, Inc.) at 37 °C. The oxygen concentration was observed using an oxygen indicator (Mitsubishi Gas Chemical Company, Inc.). The oxygen concentration in the Pouch-Bag was always kept at less than 0.1%.

Results and discussion

The supramolecular assembly, which was constructed using inorganic upconversion nanoparticles (UCNPs) coated with β -cyclodextrin-grafted hyaluronic acid (HACD) as the host and arylazopyrazole-modified spermine (AAPS) as the guest, is shown in Scheme 1. The host was synthesized *via* the ligand exchange of oleic acid (OA)-capped UCNPs (OA-UCNPs) with HACD. The obtained water-soluble HACD-UCNPs maintained the original crystallinity compared to the pristine OA-UCNPs, indicative of the high crystallinity of the resultant nanoparticles, where $d_{100} = 0.51$ nm was indexed to hexagonal NaYF₄ (Fig. S4a, ESI†). Moreover, it was found that the HACD-UCNPs had a good optical performance (Fig. S4b, ESI†). For this, the

photoluminescence spectra of the HACD-UCNPs were collected at an excitation wavelength of 980 nm, and showed three main emission peaks around 360, 450 and 480 nm, which correspond to the $^1D_2 \rightarrow ^3H_6$, $^1D_2 \rightarrow ^3F_4$, and $^1G_4 \rightarrow ^3H_6$ transitions from Tm³⁺, respectively. The ultraviolet light of about 360 nm emitted by the HACD-UCNPs can effectively induce the isomerization of AAPS from the *trans*- to the *cis*-isomer. Besides, TEM images and DLS experiments indicated that the sizes of HACD-UCNPs were about 50 nm (Fig. S5, ESI†). Because the nanoparticles were covered by negatively charged HACD, the zeta potential of the HACD-UCNPs was negative 15.93 mV (Fig. S6, ESI†). The mass ratio of HACD to UCNPs was calculated using thermogravimetric analysis (Fig. S7, ESI†), which meant that every 1 mg of UCNPs was coated with 1.48 μ mol of HACD. Moreover, the HACD covering the surface of the UCNPs not only increased water solubility of UCNPs but also could actively target cancer cells. In addition, cyclodextrins (CDs) provide cavities for the specific binding of arylazopyrazole at AAPS in which the spermine group at another terminal interacts strongly with the nucleic acids, so as to lay the foundation for regulating NAs. On the other hand, AAPS was obtained *via* simple amide condensation and removal of *t*-butoxy carbonyl reaction. Importantly, AAPS plays a key role as a bridge, connecting the HACD-UCNPs and NAs, so that this supramolecular system can perform biological functions under artificial control.

First, the molecular binding behaviour of AAPS and β -CD was studied using nuclear magnetic resonance spectroscopy (NMR) and UV-Vis spectroscopy. Compared with free *trans*-AAPS, the ¹H NMR spectrum showed that the signal of the aromatic protons in *trans*-AAPS experience a slight downfield shift after the addition of an equimolar amount of β -CD (Fig. S8, ESI†). Moreover, there was a clear correlation signal



Scheme 1 (a) Schematic and molecular structures of the AAPS-HACD-UCNPs@NAs ternary supramolecular assembly. (b) Schematic representation of manually regulated NA release *via* NIR irradiation and reductase in cells cultured under anaerobic conditions.

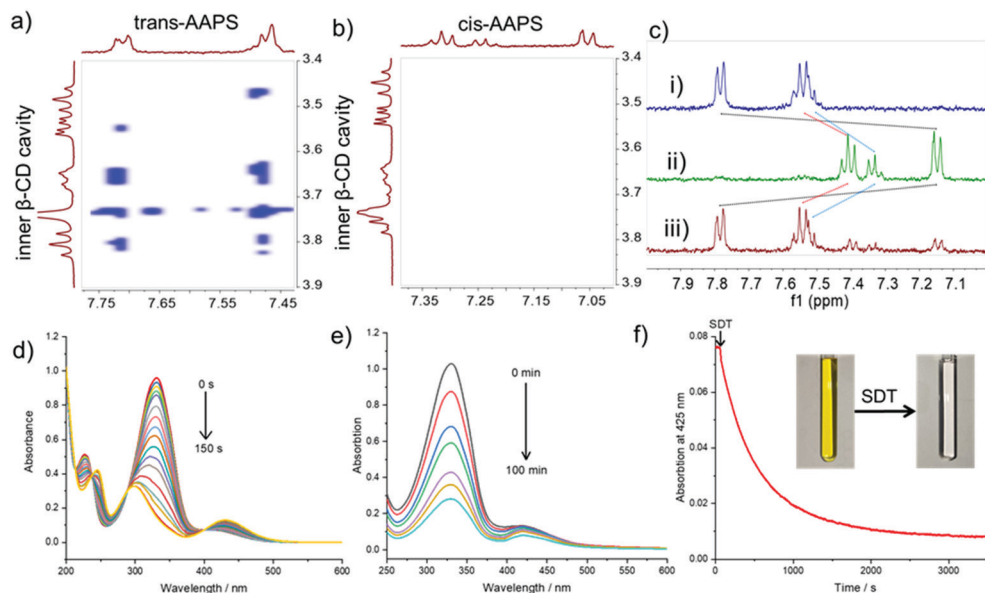


Fig. 1 Rotating frame Overhauser effect spectroscopy (ROSEY) of *trans*-AAPS (a) and *cis*-AAPS (b) with β-CD (400 MHz, D₂O, 298 K, mixing time = 0.3 s). (c) ¹H NMR spectra of AAPS-β-CD (i) before and (ii) after UV irradiation at 365 nm for 20 min, and then (iii) exposed to visible-light irradiation at 520 nm for another 10 min (400 MHz, D₂O, 298 K). (d) UV-Vis spectrum of AAPS-β-CD under 365 nm light irradiation in PBS (pH 7.2, 0.01 M, 25 °C). (e) UV-Vis spectrum of AAPS-β-CD under 980 nm light irradiation at 1 W cm⁻² in PBS ([HACD-UCNPs] = [AAPS] = 50 μM, pH 7.2, 0.01 M, 25 °C). (f) Absorbance at 425 nm of AAPS-β-CD as a function of time following the addition of SDT in PBS ([AAPS-β-CD] = 50 μM, [SDT] = 1 mM, pH 7.2, 0.01 M, 25 °C), where the insets show the optical color changes of AAPS-β-CD upon reaction with SDT.

between the protons of β-CD and the aromatic protons of *trans*-AAPS using rotating frame Overhauser effect spectroscopy (ROSEY), indicating that the benzene unit of *trans*-AAPS was inside the cyclodextrin cavity, forming the *trans*-AAPS-β-CD complex (Fig. 1a). After irradiating the *trans*-AAPS-β-CD complex using UV light (365 nm) for 5 min, the nuclear Overhauser effect (NOE) correlations disappeared between the obtained *cis*-AAPS and β-CD, showing that *cis*-AAPS escaped from the β-CD cavity (Fig. 1b). Then, the isomerization efficiency of AAPS-β-CD was quantitatively studied *via* the integral of the ¹H NMR spectrum (Fig. 1c). The conversion efficiency of the photoisomerization process for *trans*-to-*cis* and *cis*-to-*trans* could respectively achieve about 93% and about 78%, which confirmed the good photoisomerization properties of AAPS-β-CD. Thereafter, further photo-responsive properties of this supramolecular assembly were studied in phosphate buffer solution (PBS). For free AAPS, it reached a photo-steady state after irradiation at 365 nm for 180 s, while the addition of β-CD can accelerate this photoisomerization and make AAPS reach the photo-steady state with 150 s (Fig. 1d and Fig. S10, ESI†). The *trans*-*cis* photoisomerization rate constant (*k_r*) of AAPS using first-order kinetics increased from 0.035 to 0.040 s⁻¹ upon the addition of β-CD. Furthermore, the isomerization of AAPS-β-CD was monitored using UV-Vis measurements with alternating irradiation at 365 and 520 nm to determine that the reversibility and the photoisomerization properties of AAPS-β-CD did not change significantly after five cycles (Fig. S11, ESI†). Notably, the absorption peak of AAPS-β-CD around 330 nm shows a significant drop with 980 nm irradiation (Fig. 1e). Compared with irradiation at 365 nm, and despite the

isomerization induced by NIR light being slow because of the low quantum yield of upconversion, the structural switching of AAPS caused by NIR light was still effective. In comparison, the UV-Vis spectrum of free AAPS showed no obvious change under 980 nm light illumination (Fig. S12, ESI†). These experiments confirm our hypothesis that the disassembly of the supramolecular assembly, *i.e.*, the isomerization of AAPS causing it to escape from the CD cavity, can be achieved using NIR light.

On the other hand, the azo group was found to break when using a chemical reducing reagent or under a reductive micro-environment within the cells.²⁵ Considering that β-CD has a stronger affinity for the benzene unit than for the pyrazole unit covalently linked to spermine,¹⁴ the reduction cleavage of the azo bond in AAPS can also lead to the destruction of the supramolecular assembly, bringing about the release of nucleic acid. UV-Vis spectroscopy was employed to test the hypoxia response of azo group in AAPS. The *n*-π* absorption peak of AAPS at around 425 nm showed a dramatic decrease upon the addition of sodium dithionite (SDT) as a chemical azo-reducing agent (Fig. S13, ESI†). Correspondingly, the solution changed from yellow to colorless, revealing the complete reduction of the azo group. The reducing kinetics curve of the absorbance at 425 nm showed a good fit with a quasi-first-order reaction decay model (adj. *R*² > 0.996). The rate constant and half-life time were calculated to be 0.19 min⁻¹ and 3.59 min, respectively. The inclusion of β-CD slows down the reduction process of the azo unit in AAPS, reducing the rate constant to 0.12 min⁻¹ and increasing the half-life to 5.78 min (Fig. 1f and Fig. S14†). Besides, in the presence of other agents (cysteine, reduced glutathione and Na₂SO₃), there is basically no change in the

UV spectrum of AAPS, indicating that the azo bond has not been reduced (Fig. S15, ESI†).

Thereafter, we used plasmid DNA (pBR322) as the model molecule to investigate the ability of this supramolecular assembly to condense and release nucleic acids. Agar gelatin electrophoresis was carried out first (Fig. 2a and Fig. S16, ESI†). The compression of pBR322 by the supramolecular assembly exhibits concentration-dependent characteristics, which only can compress DNA at high concentrations. By contrast, neither the host (HACD-UCNPs) nor the guest (AAPS) alone can condense DNA. It is interesting that both the photo-induced isomerization of AAPS from the *trans*- to the *cis*-isomer (including UV and NIR light) and the cleavage of the azo bond caused by the reducing agent leading to the disintegration of supramolecular assembly can release the plasmid DNA. Next, with a constant concentration of pBR322, DLS experiments showed that the size of the assembly increased gradually as AAPS/HACD-UCNPs increased (Fig. S17, ESI†). The zeta potential of the assembly formed using constant pBR322 and different amounts of AAPS/HACD-UCNPs changed weakly (Fig. S18, ESI†). In addition, the transmittance of the solution of free AAPS, HACD-UCNPs or their assembly all were close to 100% in the long-wavelength region over 550 nm (Fig. 2b). Mixing pBR322 with the individual host or guest did not cause a significant change in the

transmittance, showing that there was no aggregation. However, when pBR322 was added to the binary mixture of *trans*-AAPS and HACD-UCNPs, the transmittance in the long-wavelength region was significantly decreased, indicating that the rapid aggregation of large nanoparticles occurred. After the isomerization of AAPS from the *trans*- to the *cis*-isomer or breaking of the azo bond, the transmittance increased and returned to being close to 100%, which mean that dis-aggregation had occurred. According to the corresponding dynamic light-scattering (DLS) experiments (Fig. 2c), only the hydrodynamic diameter distribution of the ternary supramolecular assembly AAPS/HACD-UCNPs@pBR322 appeared in the large-size region. Similarly, when the supramolecular assembly was treated with SDT or light irradiation, the small size distribution reappeared. More intuitively, TEM experiments showed this significant change in the supramolecular assembly behavior (Fig. 2d, S19, ESI†). Free pBR322 formed nanofibers, while the complex of AAPS/HACD-UCNPs@pBR322 assembled into nanoparticles with a diameter of about 300 nm. The disassembly of the supramolecular system, which is ascribed to changes in the structure of AAPS in response to light irradiation or SDT, was accompanied by the disappearance of aggregates. As a whole, these experimental results preliminarily confirmed that the supramolecular assembly we designed can effectively condense nucleic acids and release them in response to specific types of stimulation in buffer solution.

Encouraged by the good experimental results in the aqueous medium, we further have investigated the ability of AAPS/HACD-UCNPs to carry plasmid DNA into the cells and the gene expression *in vitro* evaluated using the enhanced green fluorescent protein (EGFP) gene as a reporter gene (Fig. 3). Because of difficulty of naked DNA to enter A549 cells, there was negligible green fluorescence when viewed using a confocal microscope. Moreover, there was scarcely intracellular green fluorescence in the groups treated with host or guest in the way that was expected (Fig. S20, ESI†). By contrast, the cells treated with the ternary assembly of AAPS/HACD-UCNPs@pEGFP showed weak green fluorescence. However, compared with stimulation alone, the coordinated dis-assembly of AAPS/HACD-UCNPs@pEGFP triggered *via* irradiation (980 nm) and reductase (anaerobic culture) caused the DNA to be released for better expression, so that significant green fluorescence was observed compared with other groups. From the statistical average fluorescence intensity in A549 cells measured using ImageJ software (ver. 1.53c),²⁶ it was confirmed that the dis-assembly of this supramolecular system responded to the relevant stimulus sharply through an increase in the fluorescence intensity demonstrating better expression of the target gene (Fig. S21, ESI†). In comparison, no clear fluorescence was observed in the 293T cells incubated with AAPS/HACD-UCNPs@pEGFP, indicating that the supramolecular assembly can target cancer cells (Fig. S22, ESI†). Those above experiments confirmed that the AAPS/HACD-UCNPs we constructed can carry pEGFP into target cancer cells rather than normal cells and release it in response to specific stimuli.

Moreover, the specific silencing of disease-causing genes through RNA interference (RNAi) using short interfering RNA

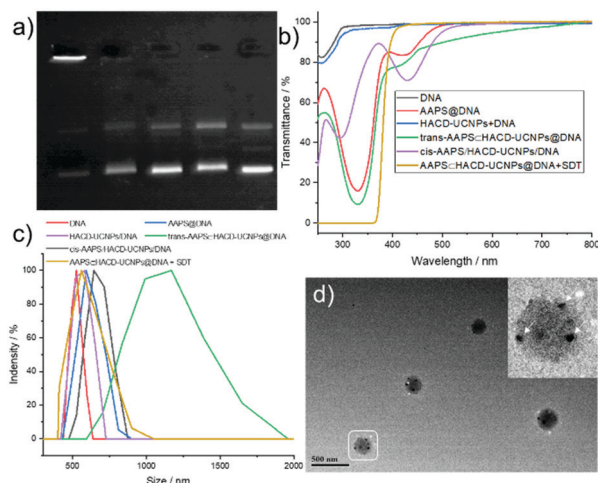


Fig. 2 (a) Agar gelatin electrophoresis (from left to right) of AAPS/HACD-UCNPs@pBR322 ([AAPS/HACD-UCNPs] = 100 μM , [pBR322] = 10 $\text{ng } \mu\text{L}^{-1}$), AAPS/HACD-UCNPs@pBR322 with 980 nm irradiation, AAPS/HACD-UCNPs@pBR322 with 365 nm irradiation, AAPS/HACD-UCNPs@pBR322 with SDT (SDT = 1 mM) and control group. (b) Optical transmittance of free pBR322 ([pBR322] = 4 $\mu\text{g mL}^{-1}$), *trans*-AAPS@pBR322 ([AAPS] = 50 μM , HACD-UCNPs/pBR322 ([HACD-UCNPs] = 50 μM), *trans*-AAPS/HACD-UCNPs@pBR322 ([AAPS/HACD-UCNPs] = 50 μM), *cis*-AAPS/HACD-UCNPs@pBR322 ([AAPS/HACD-UCNPs] = 50 μM), *cis*-AAPS/HACD-UCNPs@pBR322 with SDT (SDT = 500 μM) in PBS (pH 7.2, 0.01 M, 25 $^{\circ}\text{C}$). (c) Diameter distributions of free pBR322 ([pBR322] = 4 $\mu\text{g mL}^{-1}$), *trans*-AAPS@pBR322 ([AAPS] = 50 μM , HACD-UCNPs/pBR322 ([HACD-UCNPs] = 50 μM), *trans*-AAPS/HACD-UCNPs@pBR322 ([AAPS/HACD-UCNPs] = 50 μM), *cis*-AAPS/HACD-UCNPs@pBR322 ([AAPS/HACD-UCNPs] = 50 μM), *cis*-AAPS/HACD-UCNPs@pBR322 with SDT (SDT = 500 μM) in PBS (pH 7.2, 0.01 M, 25 $^{\circ}\text{C}$). (d) TEM image of AAPS/HACD-UCNPs@pBR322, where the inset shows an enlarged view of the supramolecular nanoparticles and the arrows indicate the HACD-UCNPs.

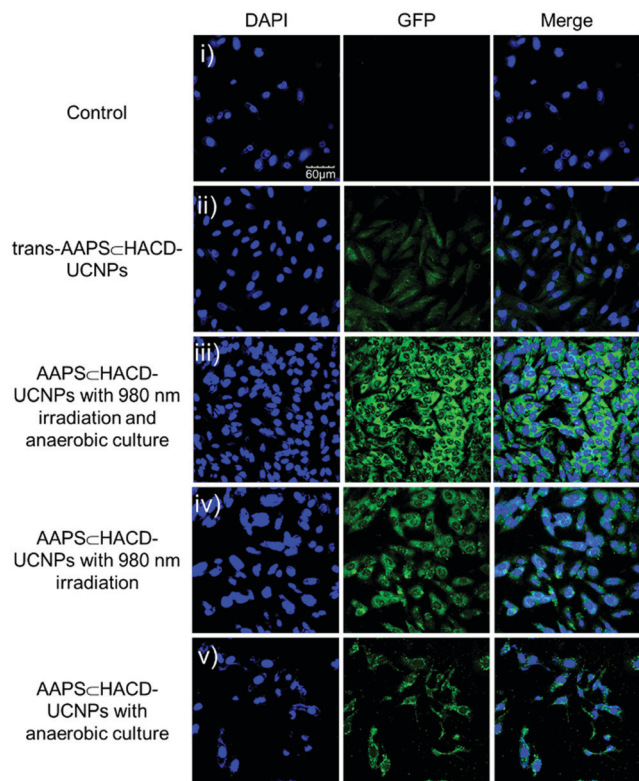


Fig. 3 Confocal laser fluorescence microscope images of A549 cells cultured with (i) free pEGFP (control), (ii) AAPS@HACD-UCNPs@pEGFP, (iii) AAPS@HACD-UCNPs@pEGFP with anaerobic culture and 980 nm irradiation, (iv) AAPS@HACD-UCNPs@pEGFP with 980 nm irradiation and (v) AAPS@HACD-UCNPs@pEGFP with anaerobic culture.

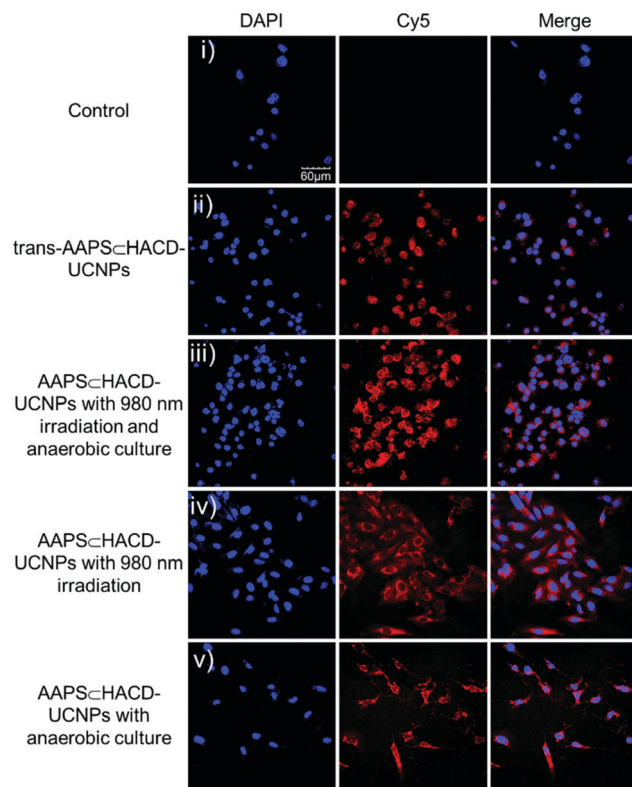


Fig. 4 Confocal laser fluorescence microscope images of A549 cells cultured with (i) free Cy5-siRNA (control), (ii) AAPS@HACD-UCNPs@Cy5-siRNA, (iii) AAPS@HACD-UCNPs@siRNA with anaerobic culture and 980 nm irradiation, (iv) AAPS@HACD-UCNPs@Cy5-siRNA with 980 nm irradiation and (v) AAPS@HACD-UCNPs@Cy5-siRNA with anaerobic culture.

(siRNA) also is a promising gene-based therapeutic strategy.²⁷ On the other hand, aerobic glycolysis (the Warburg effect) plays a vital role in the growth, metastasis, and drug resistance of cancer cells.^{28–30} Considering that cancer can be treated by regulating glycolysis *via* targeting the enzymes in that process,³¹ which was regarded as promising, glyceraldehyde 3-phosphate dehydrogenase (GAPDH), as a pivotal enzyme in glycolysis, has attracted much attention in recent years.^{31–34} Thus, we carried out siRNA transfection experiments with the assembly of AAPS@HACD-UCNPs@siRNA containing synthetic siRNA (GAPDH-homo). First, confocal laser scanning microscopy was used to certify that the supramolecular assembly could carry siRNA labeled with Cy5 fluorescent dye into the cancer cells (Fig. 4 and Fig. S23, ESI†). Specifically, A549 cells were cultured with AAPS@HACD-UCNPs@siRNA, HACD-UCNPs/siRNA, AAPS@siRNA and free siRNA, respectively. Clearly observable red fluorescence in cells treated with AAPS@HACD-UCNPs@siRNA can be seen upon the excitation at 545 nm, while there was negligible red fluorescence in cells in other cases. Furthermore, the cells cultured with AAPS@HACD-UCNPs@siRNA were further treated with irradiation (980 nm) and cultured under anaerobic conditions, which released siRNA and caused bright red fluorescence to be detected. By contrast, we cannot observe any obvious red fluorescence in 293T cells, which revealed that the siRNA entering normal cells can be

ignored (Fig. S24, ESI†). In addition, to evaluate the results of cell uptake, intracellular red fluorescence intensity was detected using a microplate reader in A549 cells treated with constant Cy5-siRNA and different amounts of AAPS@HACD-UCNPs (Fig. S25, ESI†). With the increase of the concentration of AAPS@HACD-UCNPs, the intracellular fluorescence intensity gradually increased, indicating that more siRNA entered the A549 cells. These experimental results indicated that the supramolecular assemblies can effectively carry siRNA into the targeted cancer cells.

To evaluate the gene silencing of the assembly in the cell, we performed cytotoxicity experiments with cancer cells *in vitro*. Unsurprisingly, the assembly (AAPS@HACD-UCNPs), host (HACD-UCNPs) or guest (AAPS) has no obvious toxicity toward both cancer cells (A549 and HeLa) and normal cells (293T) (Fig. 5a and S26, ESI†). The group of A549 cells cultured with AAPS@siRNA showed low cytotoxicity at high concentrations (Fig. S27, ESI†); moreover, after further irradiation or anaerobic culture, the cytotoxicity did not change significantly. For the mixture of HACD-UCNPs/siRNA, there is no effect on the growth of A549 cells at various concentrations and further treatments (Fig. S28, ESI†). By contrast, the ternary supramolecular assembly AAPS@HACD-UCNPs@siRNA inhibited the growth of about 15% A549 cell, which increased close to

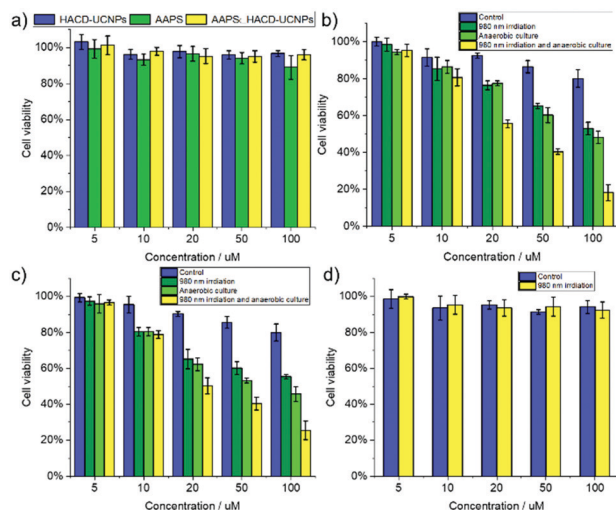


Fig. 5 (a) Cell viability of A549 cells induced with HACD-UCNPs, AAPS and AAPS-HACD-UCNPs at various concentrations; (b) cell viability of A549 cells incubated with AAPS-HACD-UCNPs@siRNA at various concentrations and with different treatments; (c) cell viability of HeLa cells incubated with AAPS-HACD-UCNPs@siRNA at various concentrations and with different treatments; and (d) cell viability of 293T cells incubated with AAPS-HACD-UCNPs@siRNA at various concentrations and with different treatments. The concentration of siRNA in all experiments was 100 nM.

47% caused by the isomerization of AAPS under 980 nm irradiation (Fig. 5b). In addition, incubation with AAPS-HACD-UCNPs@siRNA under anaerobic conditions, where the azo bond is broken by azo reductase leading dis-assembly of the supramolecular system, caused the growth of A549 cells (about 52%) to be inhibited. Favorably, combined anaerobic incubation and 980 nm irradiation inhibited the growth of most A549 cells treated with AAPS-HACD-UCNPs@siRNA (about 82%). As a negative control, the growth of A549 cells treated with AAPS-HACD-UCNPs@c-siRNA under anaerobic conditions and 980 nm irradiation was not significantly affected (Fig. S29, ESI†). By analogy, intracellular dis-assembly of the supramolecular system releasing siRNA can substantially increase the toxicity to HeLa cells (Fig. 5c). However, the cell viability of 293T cells was not significantly affected after incubation with AAPS-HACD-UCNPs@siRNA (Fig. 5d), which demonstrated the targeting ability of the supramolecular assemblies. These cell experiments confirmed that the supramolecular assemblies can effectively load siRNA into targeted cancer cells and release siRNA under corresponding stimulation to inhibit the growth of cancer cells.

Conclusions

In summary, a supramolecular carrier for the targeted delivery of nucleic acid was constructed using AAP-modified spermine and HACD-wrapped UCNPs *via* host-guest and small molecule-nucleic acid interactions. Interestingly, this supramolecular system can compress NAs and deliver them to cancer cells, and then release NAs *via* the action of NIR irradiation and

reductase under anaerobic conditions. Taking siRNA as an example, the siRNA released by the supramolecular assembly showed effective gene silencing for cancer treatment in the presence of serum. Such intelligent supramolecular carriers that are biologically non-toxic can not only achieve NA condensation but also target cancer cells, which contributes to their biodistribution and delivery *in vivo*. The stimulus responsiveness of this supramolecular system ensured the release and action of NAs at the target cells and tissues. Moving forward, effective and safe NA-delivery materials based on supramolecular chemistry show remarkable potential for gene therapy. The strategy described here has great potential for constructing intelligent biomaterials for targeted and controllable gene delivery.

Conflicts of interest

The authors declare no competing financial interest.

Acknowledgements

This work was financially supported by the National Natural Science Foundation of China (Grants 22131008).

Notes and references

- W.-C. Geng, Q. Huang, Z. Xu, R. Wang and D.-S. Guo, *Theranostics*, 2019, **9**, 3094–3106.
- E. Y. Chernikova and D. V. Berdnikova, *Chem. Commun.*, 2020, **56**, 15360–15376.
- Y.-H. Liu, Y.-M. Zhang, H.-J. Yu and Y. Liu, *Angew. Chem., Int. Ed.*, 2021, **60**, 3870–3880.
- Y.-M. Zhang, Y.-H. Liu and Y. Liu, *Adv. Mater.*, 2020, **32**, e1806158.
- S. K. Nalluri, J. Voskuhl, J. B. Bultema, E. J. Boekema and B. J. Ravoo, *Angew. Chem., Int. Ed.*, 2011, **50**, 9747–9751.
- H. Mousazadeh, Y. Pilehvar-Soltanahmadi, M. Dadashpour and N. Zarghami, *J. Controlled Release*, 2021, **330**, 1046–1070.
- J. Li, S. Xue and Z.-W. Mao, *J. Mater. Chem. B*, 2016, **4**, 6620–6639.
- X. Dai, X. Dong, Z. Liu, G. Liu and Y. Liu, *Biomacromolecules*, 2020, **21**, 5369–5379.
- Z. Liu, X. Dai, Y. Sun and Y. Liu, *Aggregate*, 2020, **1**, 31–44.
- M. E. Davis, J. E. Zuckerman, C. H. Choi, D. Seligson, A. Tolcher, C. A. Alabi, Y. Yen, J. D. Heidel and A. Ribas, *Nature*, 2010, **464**, 1067–1070.
- P. Evenou, J. Rossignol, G. Pembouong, A. Gothland, D. Colesnic, R. Barbeyron, S. Rudiuk, A. G. Marcelin, M. Menand, D. Baigl, V. Calvez, L. Bouteiller and M. Sollogoub, *Angew. Chem., Int. Ed.*, 2018, **57**, 7753–7758.
- P. Li, Y. Chen and Y. Liu, *Chin. Chem. Lett.*, 2019, **30**, 1190–1197.
- A. Tamura and N. Yui, *J. Mater. Chem. B*, 2013, **1**, 3535–3544.

- 14 L. Stricker, E. C. Fritz, M. Peterlechner, N. L. Doltsinis and B. J. Ravoo, *J. Am. Chem. Soc.*, 2016, **138**, 4547–4554.
- 15 H. Yamaguchi, Y. Kobayashi, R. Kobayashi, Y. Takashima, A. Hashidzume and A. Harada, *Nat. Commun.*, 2012, **3**, 603.
- 16 P. Shi, E. Ju, Z. Yan, N. Gao, J. Wang, J. Hou, Y. Zhang, J. Ren and X. Qu, *Nat. Commun.*, 2016, **7**, 13088.
- 17 F. Wang, Y. Zhang, Z. Du, J. Ren and X. Qu, *Nat. Commun.*, 2018, **9**, 1209.
- 18 H. Zhang, X. Fan, R. Suo, H. Li, Z. Yang, W. Zhang, Y. Bai, H. Yao and W. Tian, *Chem. Commun.*, 2015, **51**, 15366–15369.
- 19 D. Wang, M. Wagner, H. J. Butt and S. Wu, *Soft Matter*, 2015, **11**, 7656–7662.
- 20 J. Moratz, A. Samanta, J. Voskuhl, S. K. Mohan Nalluri and B. J. Ravoo, *Chem. – Eur. J.*, 2015, **21**, 3271–3277.
- 21 N. Moller, T. Hellwig, L. Stricker, S. Engel, C. Fallnich and B. J. Ravoo, *Chem. Commun.*, 2016, **53**, 240–243.
- 22 J. Liu, W. Bu, L. Pan and J. Shi, *Angew. Chem., Int. Ed.*, 2013, **52**, 4375–4379.
- 23 Y. Yang, Y.-M. Zhang, Y. Chen, J.-T. Chen and Y. Liu, *J. Med. Chem.*, 2013, **56**, 9725–9736.
- 24 T. Zhang, Z. Liu, H. Aslan, C. Zhang and M. Yu, *J. Mater. Chem. B*, 2020, **8**, 6429–6437.
- 25 W. C. Geng, S. Jia, Z. Zheng, Z. Li, D. Ding and D. S. Guo, *Angew. Chem., Int. Ed.*, 2019, **58**, 2377–2381.
- 26 C. A. Schneider, W. S. Rasband and K. W. Eliceiri, *Nat. Methods*, 2012, **9**, 671–675.
- 27 K. A. Whitehead, R. Langer and D. G. Anderson, *Nat. Rev. Drug Discovery*, 2009, **8**, 129–138.
- 28 O. Warburg, *Science*, 1956, **123**, 309–314.
- 29 M. G. Vander Heiden, L. C. Cantley and C. B. Thompson, *Science*, 2009, **324**, 1029–1033.
- 30 B. J. Altman, Z. E. Stine and C. V. Dang, *Nat. Rev. Cancer*, 2016, **16**, 619–634.
- 31 H. Pelicano, D. S. Martin, R. H. Xu and P. Huang, *Oncogene*, 2006, **25**, 4633–4646.
- 32 C. Guo, S. Liu and M. Z. Sun, *Clin. Transl. Oncol.*, 2013, **15**, 167–172.
- 33 J. Yun, E. Mullarky, C. Lu, K. N. Bosch, A. Kavalier, K. Rivera, J. Roper, I. I. Chio, E. G. Giannopoulou, C. Rago, A. Muley, J. M. Asara, J. Paik, O. Elemento, Z. Chen, D. J. Pappin, L. E. Dow, N. Papadopoulos, S. S. Gross and L. C. Cantley, *Science*, 2015, **350**, 1391–1396.
- 34 M. D. Kornberg, P. Bhargava, P. M. Kim, V. Putluri, A. M. Snowman, N. Putluri, P. A. Calabresi and S. H. Snyder, *Science*, 2018, **360**, 449–453.